RSC Advances

PAPER

View Article Online
View Journal | View Issue



CrossMark click for updates

Cite this: *RSC Adv.*, 2016, **6**, 6686

# Sulfated zirconia foams synthesized by integrative route combining surfactants, air bubbles and sol–gel transition applied to heterogeneous catalysis†

Marinalva A. Alves-Rosa,* Leandro Martins, Peter Hammer, Sandra H. Pulcinelli and Celso V. Santilli

Received 18th November 2015
Accepted 7th January 2016

DOI: 10.1039/c5ra24413g

www.rsc.org/advances

Sulfated zirconia ceramic foams were produced by the sol–gel process using air–liquid foam and surfactants as dual pore templates. The results showed the presence of high porosity (until 93%) and surface area (105 $m^2\ g^{-1}$), and a hierarchical structure of pore sizes in the range of macro (between 10 and 76 μm), and meso-scales (≅6 nm). The hierarchical porous structure and pore wall texturization of ceramic foams produced by this process, besides the presence of strong acid sites, certify these materials as heterogeneous catalysts for dehydration reactions.

## 1. Introduction

Ceramic foams presenting a multimodal pore size distribution with a hierarchical structural arrangement of micro, meso and macropore families have attracted great interest in the last decade.[1–3] Each hierarchical structural level assumes different functions in the material.[2] For example, in catalytic applications the macropores (>50 nm) facilitate mass transfer, reducing transport limitations, while the mesopores (2–50 nm) and micropores (<2 nm) host the active sites for catalytic reactions, acting as functional environments when a high surface area is necessary.[2,4]

The integration of the sol–gel process with structural templates such as air–liquid foams and biliquid foams, among others, is emerging as a broad area of research and offers the possibility of achieving new architectures at various length scales with enhanced properties.[5,6] Specific porous structures can be tailor made for a given application. This is directly related to the fine-tuning of synthesis parameters and to the routes of ceramic foams preparations. There are several foaming procedures in use, for example, gelcasting,[7] preceramic polymers[2] and sol–gel process.[8,9] The process involving the direct foaming of the gel has demonstrated to be the most efficient, due to the easy workability associated to the one-pot synthesis. The use of foaming agents or surfactants to create air bubbles is necessary in these processes, as they stabilize the air–liquid interface. After the gelation and trapping of air-bubbles, the foamed gel is dried and fired in order to convert the xerogel into ceramic foam.[10,11]

The preparation of meso and macroporous ceramic materials usually uses surfactants to produce the pores. These surfactants can be non-ionic,[9] cationic[12] and anionic.[11,13] Several studies have been carried out focusing the kind of surfactant that better stabilizes the foamed gel to produce the ceramic foam with desired structural properties.[14,15] The use of surfactants allows the dual templating by micelle and gas bubbles and the production of the macro and mesopores in the final ceramic material according to the steps depicted in Scheme 1.

Compared to other solid acid catalysts sulphated zirconia has usually a low surface area. However, sulfated zirconia samples are recognized as superacidic catalysts which has attracted a great deal of interest.[16–18] Numerous studies have been devoted to the preparation of these catalysts and to their application in several reactions such as alkane isomerization in gas phase,[19] and esterification of benzoic acid to methylbenzoate in liquid phase,[20] dehydration reaction[17,21] and others reactions of industrial interest.[16] Therefore, any improvement in the generation of pores and specific area is highly welcome to increase the overall performance of these catalysts.

In this work the sol–gel transition and air–liquid foams were used to produce hierarchical structure of pores in sulfated zirconia ceramic foams in the presence of different surfactants. The ceramics that present high values of surface area and pore volume are interesting for the application in heterogeneous catalysis. Under this perspective, the catalytic activity of the ceramic foams was evaluated using the ethanol dehydration reaction as a function of the presence of Brønsted and Lewis acid sites, and the effects of porosity, surface area and sulfur content on the porous zirconia ceramics were discussed.

*Univ Estadual Paulista/Unesp, Institute of Chemistry, P.O. Box 355, Araraquara 14800-900, Brazil. E-mail: nalva@iq.unesp.br; Fax: +55-016-3322-2308; Tel: +55-016-3301-9766*

† Electronic supplementary information (ESI) available: Pore size distribution, mapping of sulfur content, representative structure of the sulfated zirconia and selectivity of the ceramic foams on reaction of ethanol dehydration. See DOI: 10.1039/c5ra24413g

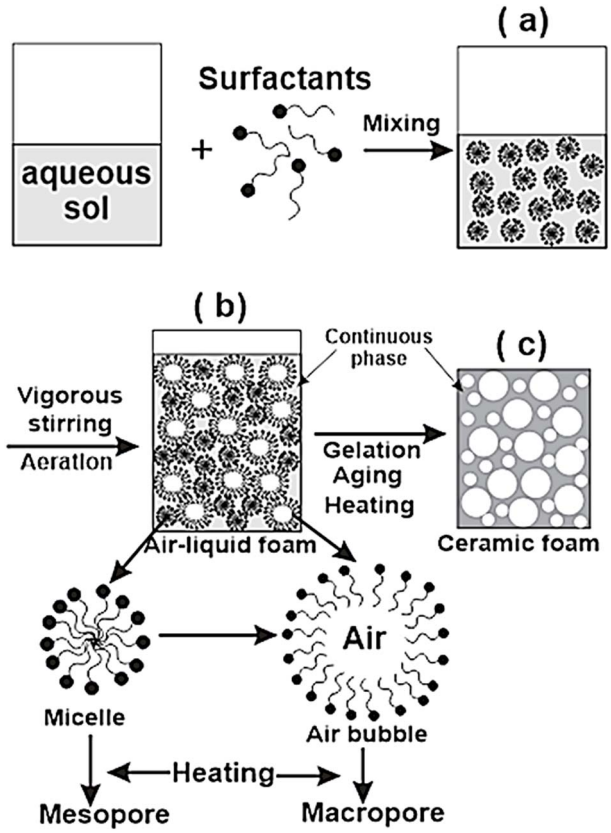


Scheme 1 Design of the steps used to obtain macro–mesopores in ceramic materials through air–liquid foaming process: (a) surfactant micelles stabilized in a sol, (b) micelles surfactant and air bubbles insertion by aeration under stirring, (c) bimodal porous ceramic obtained after gelation, aging, drying and firing.

## 2. Experimental

### 2.1 Preparation of sulfated zirconia ceramic foams

The sulfated zirconia hydrosol was prepared by the procedure previously described,[22] consisting of the following steps: dissolution of $ZrOCl_2 \cdot 8H_2O$ (Aldrich) in water (1.5 mol $L^{-1}$) followed by the addition to a hot (80 °C) aqueous sulfuric acid solution (1.5 mol $L^{-1}$), until reaching a proportion of $Zr^{4+} : SO_4^{2-} = 15 : 1$. The colloidal suspension was cooled to room temperature (25–28 °C) and dialyzed against bidistilled water for 24 h. The Zr concentration was increased from 0.5 to 3.5 mol $L^{-1}$ by solvent evaporation at 55 °C using a rotating evaporator. In a second step, the gelation was induced by adding sulfuric acid to this clear sol until reaching $Zr^{4+} : SO_4^{2-} = 3 : 1$.

The preparation[8,10] of the foams from the transparent aqueous sol of sulfated zirconia consisted in their aeration under vigorous and constant stirring (2000 rpm) in presence of four different surfactants at constant weight (10 wt%): (1) anionic sodium dodecylsulfate (SDS); (2) cationic octadecyltrimethylamonium bromide (OTAB); (3) non-ionic block copolymer poly(oxyetylene)–poly(oxypropylene)–poly(oxyetylene) PLURONIC F-127 and (4) nonylphenol ethoxylate, commercially known as IGEPAL 850®. The concentrations of the surfactants were used above the Critical Micellar Concentration (CMC) and the respective values in mol $L^{-1}$ are: SDS – 0.62; OTAB – 0.45; PLURONIC 0.014 and IGEPAL 0.16. Gelation of the foamed sol occurred a few minutes after the addition of sulfuric acid. In order to improve the viscoelastic properties, the gel foams were aged at room temperature in closed flasks for 9 days. The conversions of the gel to xerogel and then to ceramic were carried out by drying at 55 °C for 48 h and firing at 600 °C for 2 h in a muffle oven, respectively. A reference sample, denoted as SZr-ref, was prepared following the same procedure but in absence of surfactants in order to compare their additive contributions to porosity.

### 2.2 Chemical, structural and porous properties characterization

The effect of the surfactant (anionic, cationic or non-ionic) in the foams microstructures was analyzed by skeletal ($\rho_s$) and bulk ($\rho_b$) density, measured by Helium (AccuPycc 1330, Micromeritics) and Dried-Fluid® (GeoPyc 1360, Micromeritics) picnometry, respectively. The open porosity ($P$) was calculated based on the measured density values by using the relation $P = (1 - \rho_b/\rho_s)$. The macropore size distribution of the ceramics was determined from mercury intrusion porosimetry using the AUTOPORE III equipment (Micromeritics). The pore diameter was calculated from Washburn equation,[23] using surface tension and contact angle of 0.489 N $m^{-1}$ and 135°, respectively. BET surface areas were estimated by nitrogen adsorption/desorption isotherms recorded on a Micromeritics (ASAP 2010) equipment and the mean mesopore size (d) was determined by the relationship between the BET area ($A_{BET}$) and the pore volume ($V_p$) at relative pressure of 0.98 as $d = 4V_p/A_{BET}$.[24] The isotherms were recorded at liquid nitrogen temperature and relative pressure interval between 0.001 and 0.998; the samples were evacuated prior to measurements at 200 °C for 12 h under vacuum of $\sim 1 \times 10^{-2}$ Pa. Scanning electron micrographs were recorded using a Philips XL 30 equipment. The samples were deposited in an aluminum sample holder and sputtered with gold.

The crystalline structure of the calcined samples was analyzed by X-ray powder diffraction (XRPD). The data were collected on a Siemens D-5000 diffractometer, using the Cu K$\alpha$ radiation monochromatized with a curved graphite single-crystal and a $2\theta$ interval between 5° and 80°. The crystalline tetragonal phase quantification and identification of the sulfated zirconia foams was performed using eqn (1) and the JCPDS crystallographic pattern files [79-1771] and [83-0943] for tetragonal and monoclinic phases, respectively[21]

$$\%\ \text{tetragonal} = \left[\frac{I_{T(101)}}{I_{T(011)} + \left(I_{M(-111)} + I_{M(111)}\right)/2}\right] \times 100 \quad (1)$$

where $I_{T(101)}$ is the integrated intensity of (1 0 1) peak of tetragonal phase and $I_{M(-111)}$ and $I_{M(111)}$ are the integrated intensity of (−1 1 1) and (1 1 1) peaks of monoclinic phase, respectively.

Thermogravimetric measurements were carried out to quantify the amount of sulfur present in the sulfated zirconia

samples after firing at 600 °C. The experiments were performed in SDT Q600 Simultaneous TG/DTA equipment from TA Instruments. The samples were heated from room temperature at a rate of 10 °C $min^{-1}$ under oxygen flow (100 $cm^3$ $min^{-1}$) up to 1000 °C. The sulfur concentration was determined by correlating the weight loss with the stoichiometric release of sulfur as $SO_3$.

The X-ray photoelectron spectroscopy (XPS) measurements were carried out using a commercial spectrometer (UNI-SPECS UHV). The Mg Kα line was used ($h\nu$ = 1253.6 eV) and the analyzer pass energy was set to 10 eV. The binding energies of the Zr 3d, S 2p, and O 1s core level spectra were corrected using the hydro-carbon component of adventitious carbon fixed at 285.0 eV. The composition of the surface layer was determined from the ratios of the relative peak areas corrected by sensitivity factors for the corresponding elements. The deconvoluted spectral components were obtained using multiple Voigt profiles (70% Gaussian and 30% Lorentzian), without placing constraints. The width at half maximum (FWHM) varied between 1.5 and 2.2 eV, and the accuracy of the peak positions was ±0.1 eV.

### 2.3 Catalytic dehydration of ethanol

The ethanol dehydration was performed in a plug flow reactor fitted with a thermocouple extending to the center of the catalytic bed. The data were collected under atmospheric pressure using 100 mg of catalyst. Liquid ethanol (99.8% Merck) was pumped into the heated reactor (1 mL $h^{-1}$ or 17.1 mmol $h^{-1}$) using a syringe pump and a flow of 25 mL $min^{-1}$ of nitrogen measured by a mass flow controller fed as a carrier gas. The composition of the reactor effluent stream was analyzed using a gas chromatograph (CG) equipped with a flame ionization detector (FID) connected online to the reactor outlet. A DB-1 capillary column was used in the analysis of the product stream. Ethene, acetaldehyde, ethanol and diethyl ether were recorded in GC analysis and the calibration was performed using a mixture of reactant and products of known composition. Before each experiment, the catalyst was dried at 200 °C *in situ* under nitrogen stream. Data were collected every 7 min while the reaction temperature was increased from 150 to 300 °C in steps of 50 °C. Each data point corresponds to an average of results obtained for at least four successive measurements under isothermal conditions.

## 3. Results and discussion

### 3.1 Porosity characterization

The macroporosity of the foams prepared by the aeration of the zirconia sol using different surfactants was characterized by mercury intrusion porosimetry as shown in Fig. 1. The cumulative pore size distribution (Fig. 1(a)) evidences the higher pore volume of macropores with similar average sizes for the ionic (SDS – 12 μm and OTAB – 10 μm) and non-ionic (IGEPAL – 73 μm e PLURONIC – 76 μm) surfactants. The SZr-ref shows a family of small pores centered at around 0.10 μm with a total pore volume of only 0.1 $cm^3$ $g^{-1}$. This additive effect of the

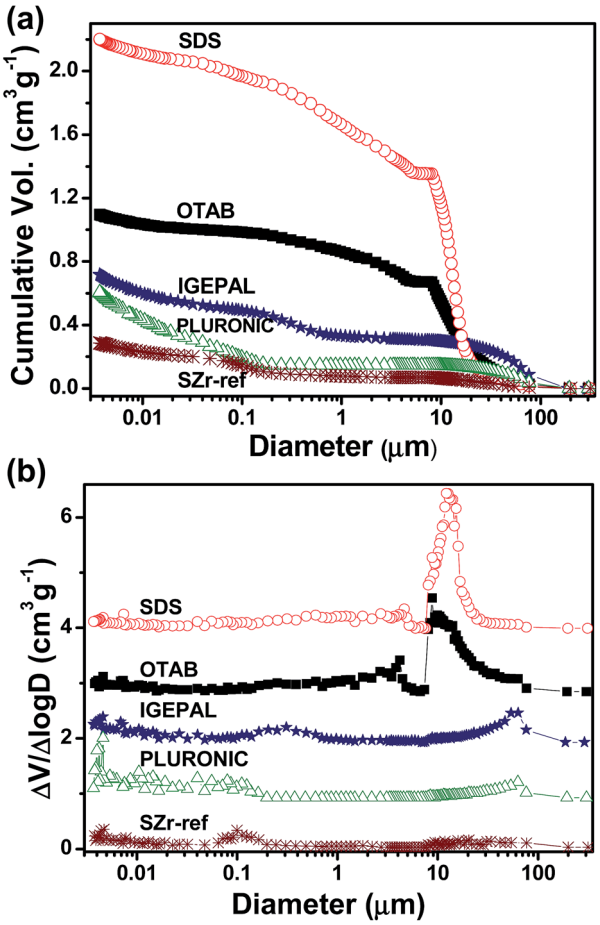


Fig. 1 Effect of the different surfactants on the (a) cumulative pore volume and (b) differential pore size distribution of the final ceramic foam.

surfactants is due to the sol–gel transition combined with foaming of gelled samples that entraps the air bubbles and micelles inside the gel network, which forms inverse replicas after the elimination of the solvent in the succeeding drying and firing steps.[25] The high quantity of macropores in the sample prepared with SDS allows for the higher pore volume observed in this case (2.2 $cm^3$ $g^{-1}$). This porosity could be a consequence of the higher amount of SDS molecules (high molar concentration) and the xerogel monolithicity visually observed by the full maintenance of the ceramic body, characterized by the preservation of the initial cylindrical shape, and shrinkage of less than 5% during the gel–xerogel conversion. On the other hand, the fired SZr-ref sample showed up as a dense monolithic body as result of a drying shrinkage of ≈40% verified under absence of surfactants. The OTAB, IGEPAL and PLURONIC ceramic foams presented linear shrinkage of about 15% during the gel–xerogel conversion preserving part of their monolithic bodies (≅50% of the initial bulk), however exhibiting an intermediate behavior between the extreme porous characteristics of SDS foamed ceramic and SZr-ref sample. The SDS surfactant acts more effectively in the formation of the liquid foam because the presence of the electric double layer stabilizes the air–liquid interface, favoring the mechanic stability and

 

preventing the coalescence of the air bubbles. Non-ionic surfactants are generally less efficient in foaming of aqueous solution, because they have rather larger molecular surface areas, which hinders the lateral interaction of the adsorbed molecules, resulting in a poor interfacial elasticity of the liquid foams.[26]

The pore size distribution showed in the Fig. 1(b) points a main pore family in the region of macropores for the samples synthesized in the presence of ionic surfactants. The average size of pore families, determined from mercury intrusion and nitrogen physisorption, surface area and porosity of all foamed ceramics are presented in Table 1. The difficulty to reach a narrow pore size distribution in samples SDS and OTAB is due to the high quantity of air bubbles introduced in the liquid foam or/and to processes such as coalescence and coarsening which changes the bubbles size. An intermediary pores family is observed between the macro and the mesopores with a broad pore size distribution, presenting larger sizes (0.2–4.6 μm) for samples foamed with ionic surfactant (SDS and OTAB) and smaller sizes (0.04–0.3 μm) for the samples prepared with non-ionic surfactants (PLURONIC and IGEPAL). The minimum value in the bulk density (0.38 g $cm^{-3}$) and the maximum value of porosity (93%) were obtained for the sample prepared with SDS, because of the higher efficient liquid foaming and low post-synthesis shrinkage. The porosity decreases from ionic to non-ionic surfactants, and the opposite occurs with the surface area. The ceramic foams prepared with SDS and PLURONIC have surface areas of 5 and 105 $m^2$ $g^{-1}$, respectively. The total pore volume obtained by picnometry is directly related to the porosity and corresponds to the higher volume for foam prepared with SDS (2.2 $cm^3$ $g^{-1}$) and to the smaller one for foam prepared with PLURONIC surfactant (0.6 $cm^3$ $g^{-1}$). Thus, there is no direct relationship between the pore volume and the surface area, because the pore volume is dependent of the maintenance of macroporous structure of the foam during ceramic conversion, while the surface area depends on the presence of micro and mesopores. As expected in SZr-ref, the porous characteristics are poor, with low porosity and total pore volume and high bulk density. The surface area of the SZr-ref sample was slightly higher than the SDS, pointing out that the SDS changes the structure of the sulfated zirconia precursor. The sulfate ion and its anionic counter ion in the molecule of SDS can interact with the oligomeric structures of the zirconia sol,[25] modifying the initial configuration of the material and affecting the structure of the foam.

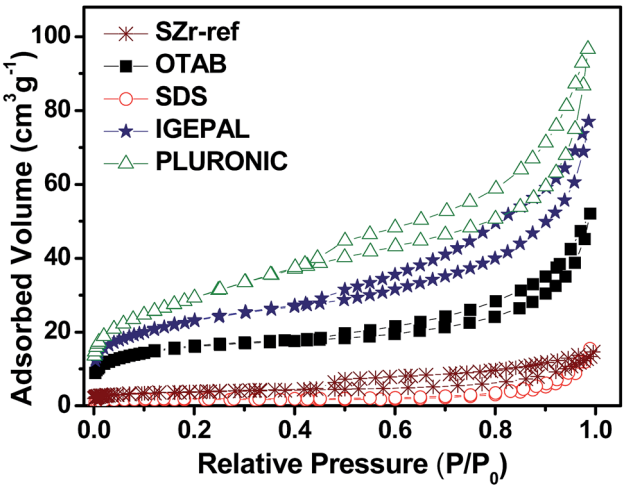


Fig. 2 Nitrogen adsorption–desorption isotherms of the ceramic foams prepared with different surfactants.

The nitrogen adsorption–desorption isotherms of the foamed samples with different surfactants are presented in the Fig. 2. The hysteresis loop between the adsorption and desorption branches is characteristic of mesoporous materials with pore sizes smaller than 50 nm.[24] However, the absence of a plateau in the relative pressure close to 1 is typical of type II isotherms, which are frequently observed for macroporous solids with pore sizes larger than 50 nm.[24] Therefore, the presence of both features hints on the coexistence of mesopores and macropores, in good agreement with the pore size distribution revealed by Hg porosimetry (Fig. 1(a)). The absence of hysteresis loop for the sample prepared with SDS and SZr-ref confirms the absence of mesopores. The shape of the hysteresis loop is in accordance with the H3 type of IUPAC classification, usually associated to slit-shaped pores formed by platelet aggregation resulting in large pores size distribution.[24] The mean mesopore size was determined by the ratio $4V_p/A_{BET}$ encompassing the different geometric pores format.[24] A mean diameter around 6 nm was observed for samples prepared with OTAB, IGEPAL and PLURONIC (Table 1), indicating no influence of the surfactant in this pore family. The pore size distribution using

Table 1 Porous characteristic of the zirconia foams prepared with different surfactants

| Sample | Total pore volume ($cm^3$ $g^{-1}$) | Bulk density (g $cm^{-3}$) | Porosity (%) | Mean macropore size[a] (μm) | Mean mesopore size[b] (nm) | Surface area $A_{BET}$ ($m^2$ $g^{-1}$) | Mesopore volume $V_p$ ($cm^3$ $g^{-1}$) |
|---|---|---|---|---|---|---|---|
| SZr-ref | 0.12 ± 0.01 | 2.61 ± 0.01 | 32 ± 1 | 0.10 | — | 13 ± 1 | 0.012 |
| SDS | 2.20 ± 0.12 | 0.38 ± 0.02 | 93 ± 4 | 12.3 | — | 5 ± 1 | 0.024 |
| OTAB | 1.10 ± 0.01 | 0.52 ± 0.01 | 90 ± 1 | 10.1 | 6.1 | 53 ± 3 | 0.081 |
| IGEPAL | 0.71 ± 0.03 | 0.60 ± 0.01 | 86 ± 2 | 73.2 | 6.0 | 79 ± 4 | 0.12 |
| PLURONIC | 0.60 ± 0.01 | 0.74 ± 0.01 | 75 ± 1 | 76.5 | 5.7 | 105 ± 5 | 0.15 |

[a] Pore sizes determined from mercury intrusion porosimetry. [b] Pore sizes determined from $D_{mesopore} = 4V_p/A_{BET}$ from the nitrogen physisorption isotherms.

the BJH method for the desorption branch was included in the ESI (Fig. S1†) for supporting the values of mean mesopores size showed in the Table 1.

The microstructural characteristics of ceramic foams prepared with different surfactants was analyzed by scanning electron microscopy (SEM) (Fig. 3). Foams prepared with SDS and OTAB have spherical macropores of variable size between 10 and 60 μm, presenting textured walls (Fig. 3(a) and (b)) and are free of cracks. On the other hand, IGEPAL (Fig. 3(c)) and PLURONIC (Fig. 3(d)) caused the formation of macropores with textured walls in a smaller order of magnitude than the latter ones. The pore wall texture observed in this case results from disordered packing of platelets, which is in good agreement with the existence of slit-shaped pores indicated by H3 type hysteresis loop (Fig. 2). The visualization of surface texture of sample SZr-ref confirms the non-parallel packing of platelet in the pores walls is characteristic of the sulfated zirconia precursor.[25] Macropores are not visualized in the sample SZr-ref (Fig. 3(e)), only a textured structure that results in low pores volume measured by mercury porosimetry. The observation of sample SZr-ref with higher magnification (Fig. 3(f)) shows the presence of textured surface with pores size of same magnitude revealed by the increasing mercury intrusion between 0.005 and 0.1 μm in Fig. 1(a) observed for all the studied samples.

### 3.2 Structural and chemical characterization

The zirconium oxide has three different crystalline phases, that suffer the sequential transitions of monoclinic → tetragonal → cubic with the increasing of the temperature.[27] The uses of some aliovalent cations to replace zirconium atoms in substitutional solid solution and to form oxygen vacancies or the stabilization of nanoscopic $ZrO_2$ grains by surface modification can stabilize the high temperature cubic and tetragonal phases.[28] In the latter case sulfate anions chemisorbed in the fine $ZrO_2$ powder are usually used to raider the nanoscopic grain grow in order to obtain metastable tetragonal phase, that provides a specific catalytic performance improvement when compared to the monoclinic structure, due to the accumulation of anionic vacancies on the particles surface.[21] The tetragonal $ZrO_2$ phase is desirable for the design of supports used in redox reactions due to the improved oxygen exchange, as for example in $MoO_x$ impregnated $ZrO_2$.[29] Despite of this important property of zirconium oxides, the catalysts studied herein were assessed in the ethanol dehydration in which the redox properties are not required.

The X-ray diffraction patterns of the ceramic foams samples displayed in Fig. 4 evidences a mixture of tetragonal and monoclinic phases. The percentage of tetragonal phase ranging from 68 to 94% can be due to the different amounts of sulfate groups in samples prepared with different surfactants. The SZr-ref sample showed a smaller fraction of the tetragonal phase than the others samples, evidencing that the pore creation probably hinders the grain growth favoring the stability of the tetragonal phase, which has a lower surface energy. The presence of high percentage of tetragonal phase indicates that the thermal treatment at 600 °C does not remove a significant fraction of surface sulfate groups from the zirconia foam, which can act as Brønsted and Lewis acid sites like the observed in sulfated zirconia catalyst.[30]

The acidity and consequently activity of sulfated zirconia catalysts is influenced by two main factors, the calcination temperature and the nature of precursors used to produce the gel.[31] The calcination temperature directly affects the concentration of sulfate groups. The thermogravimetric curves displayed in Fig. 5 correspond to the ceramic foams previously treated at 600 °C and therefore, the registered weight losses are not due to firing of surfactants but related to the release of $SO_x$ species of the sulfate groups above 650 °C.

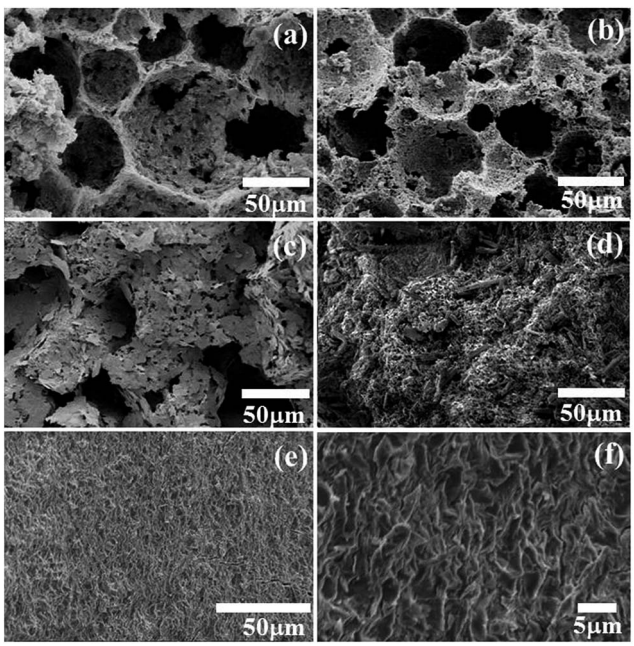


Fig. 3 Scanning electronic microscopy image from samples prepared with different surfactants: (a) SDS; (b) OTAB; (c) IGEPAL; (d) PLURONIC; (e) SZr-ref and (f) SZr-ref at higher magnification.

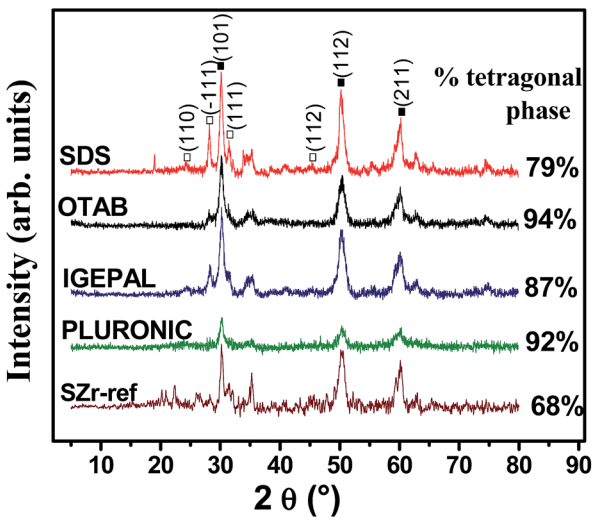


Fig. 4 XRD patterns of the zirconia samples foamed with different surfactants, ■ tetragonal phase and □ monoclinic phase.

The small weight loss bellow 110 °C is due to the desorption of surface physisorbed water. The broadening of the dTG peak (Fig. 5(b)) mainly due to the shoulder at the low temperature side and the low temperature shift in the weight loss of the surfactant foamed ceramics suggest the existence of different families of sulfate groups (tridentate, bidentate or monodentate)[25] and consequently acid sites of different strengths. The causes of these differences can be associated to the nature of sulfate $SO_x$ groups and density of surface occupancy. Sulfate groups are totally removed above 800 °C, decreasing considerably the zirconium atoms acidity. The uphold of the sulfate groups in these catalysts calcined at 600 °C is therefore important for the control of the surface acidity.[32] Although samples treated at 800 °C were not investigated in this study, one could profit from the unique porous characteristic of the support and impregnate it with active metal atoms for use in a variety of other catalytic processes.[33]

The chemical composition of the samples determined by TGA and quantitative XPS analysis, shown in Table 2, are somehow congruent between themselves. Although the bulk chemical composition of the foams varied from 1 to 9 wt%, the surface chemical composition determined by XPS varied only between 3 and 7 wt%, as a consequence of a more homogeneous density of surface acid sites.[34] The atomic S/Zr ratio of IGEPAL and OTAB foamed ceramics was maintained at around the initial ratio used in the synthesis mixture of 0.3, but there are significant variations in SDS and PLURONIC foamed samples. Mapping of sulfur, zirconium and oxygen content is provided in Fig. S2 of the ESI.† The images reveal that sulfur is homogeneously distributed on the surface of the catalysts and the sulfur amounts are close to the observed in TGA and XPS.

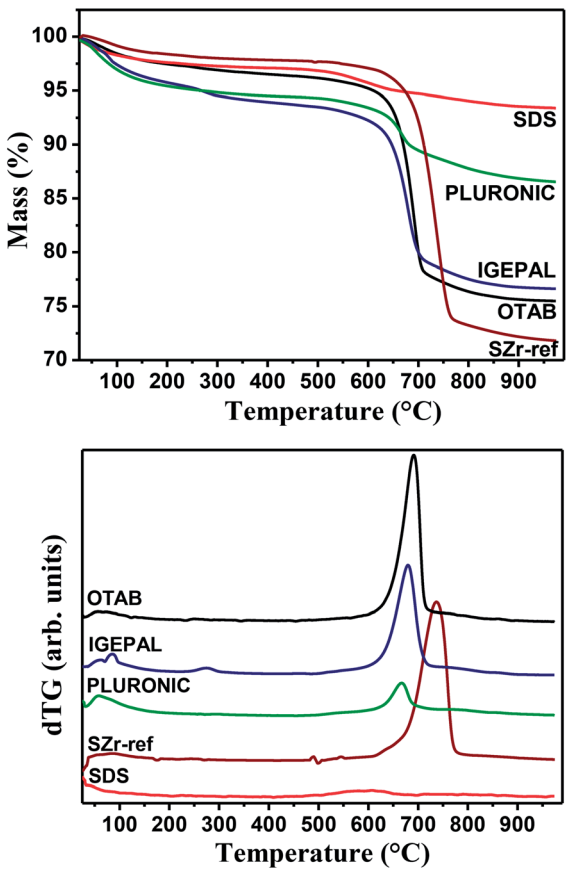


Fig. 5 Thermogravimetric curves (TG/dTG) for foams treated at 600 °C.

The knowledge of the composition and local bonding structure of the catalyst surface is essential for a consistent interpretation of the catalytic activity of the material. XPS analysis was used to get a better comprehension of the surface chemistry of the catalysts. The analysis was focused on the O 1s core-level spectra (Fig. 6(a)–(e)) and on the Zr 3d doublet of the PLURONIC sample (Fig. 6(f)), representative of all the samples, respecting their distinct proportions of sulfate. The results provided additional information on the presence of sulfate and hydroxyl groups on the catalyst surface. The quantities of the species analysed are indicated by types (1), (2) and (3), and an idealized structure is shown in the Fig. S3 of the ESI.† The hydroxyl groups are related to the Brønsted sites on the surface of the catalyst (specie type (2) in Table 2), and the sulfate groups to the Lewis sites (type (1)). The presence of these acid sites results in the remarkable acidity on the surface.[31] The deconvolution of the O 1s spectra into five components, depicted in Fig. 6(a)–(e), provided the relative amount of oxygen present in sulfate groups (532.3 eV), superficial hydroxyl groups (531.6 eV) and oxygen of the zirconium oxide bulk (530.5 eV). The weak intensities of carboxilated groups (O–C and O–C=O) at higher binding energies, related to adventitious carbon, were not included in the percentages, presented in the Table 2. In the Zr 3d spectrum (Fig. 6(f)), the two chemical environments were assigned to the $ZrO_2$ phase (182.4 eV) and to the superacid Lewis type sulfated zirconium sites (183.3 eV).[35] The chemical shift to higher binding energy is due to an electron-deficiency of the lattice zirconium atoms. On the other hand, the hydroxyl groups (O 1s) are the acid sites of the Brønsted type. Unmodified zirconium oxides are known as amphoteric compounds, because they can react as a weak acid due to framework zirconium cations as well as a weak base due to oxygen anions. Despite of the prevailing surface acidity of the catalysts, the oxygen anions of the zirconium oxide bulk remain as weak basic groups, located at a binding energy of 530.5 eV (O 1s).

### 3.3 Catalytic activity on ethanol dehydration

As discussed before, the presence of sulfate groups on the structure of the zirconia foams maintains a high amount of tetragonal phase and provides a high quantity of acid sites that might improve the catalytic performance of zirconia in several reactions. For example sulfated zirconia shows an exceptional catalytic activity at reasonably low temperatures for the conversion of several hydrocarbons of industrial interest.[16] Based on the unique combination of strong acid sites and the textural characteristic given by the microstructure of interconnected macro and mesopores, the sulfated zirconia foams synthesized herein should provide enhanced catalytic activity for a number of catalytic applications.

As an application case, the ethanol dehydration was used to evaluate the catalytic and acid properties of the zirconia

Table 2 Sulfur content determined by TGA and XPS, and the corresponding surface speciation based on O 1s binding energy

| | Sulfur wt% determined by | | Surface oxygen speciation determined by XPS[b] (%) | | |
|---|---|---|---|---|---|
| Sample | TGA[a] | XPS | (1) $ZrO_x$–$SO_4$ (532.3 eV) | (2) $ZrO_x$–OH (531.6 eV) | (3) $ZrO_2$-bulk (530.5 eV) |
| SZr-ref | 9.3 | 7.6 | 37 | 20 | 43 |
| SDS | 0.7 | 3.4 | 62 | 10 | 28 |
| OTAB | 7.3 | 5.2 | 46 | 19 | 35 |
| IGEPAL | 5.8 | 5.5 | 45 | 18 | 37 |
| PLURONIC | 1.7 | 3.5 | 58 | 16 | 26 |

[a] Weight percentage of sulfur content estimated considering the stoichiometry decomposition $SO_2 + \frac{1}{2}O_2$. [b] Surface oxygen speciation not considering adsorbed carboxylated compounds.

foams.[4,21] Ethanol can undergo intra and intermolecular dehydration on acid sites and dehydrogenation on basic sites.[4] Dehydrogenation reaction produces acetaldehyde, while dehydration produces diethyl ether at low temperatures or ethene predominantly at high temperatures.[33] Ethene is produced by the surface adsorption of ethanol molecule followed by the OH bond rupture on the acid site to give rise to a surface ethoxy group. The dehydration involves the presence of acid and basic sites of balanced strength. Diethyl ether formation from ethanol involves the reaction between two alcohol molecules chemisorbed on neighboring sites. One alcohol molecule adsorbs on an acid site through the oxygen atom from the OH group, and the alpha carbon atom becomes slightly positive. The other ethanol molecule performs a nucleophilic attack on the alpha C atom of the first molecule (through the OH group) to form diethyl ether.[28] Acetaldehyde is produced by a dehydrogenation reaction due to the presence of the basic and acid sites.

Fig. 7 shows ethanol conversion in different temperatures by the sulfated zirconia foams prepared using different surfactants. The combination of three properties of these catalysts, namely the surface area, the porosity and the acidity induced by the presence of sulfate groups (Tables 1 and 2) influenced the catalytic performance of the foams. Distinct behaviors for two groups of samples could be observed. Firstly, a very low catalytic activity was found for SZr-ref and SDS samples. Despite of the high sulfur content of SZr-ref, pointed by the TG (9.3%) and XPS (7.6%) measurements, the low surface area (13 $m^2\ g^{-1}$) and porosity difficult the access to these sites. The SDS catalyst has high porosity, but small surface area (4.9 $m^2\ g^{-1}$) and low sulfur concentration (0.7 and 3.4%), which results in a poor catalytic performance. The second group represents samples with high catalytic activity. OTAB and IGEPAL show similar activity, which can be related to their elevated porosity, surface area and sulfur content. These latter samples, OTAB and IGEPAL, were

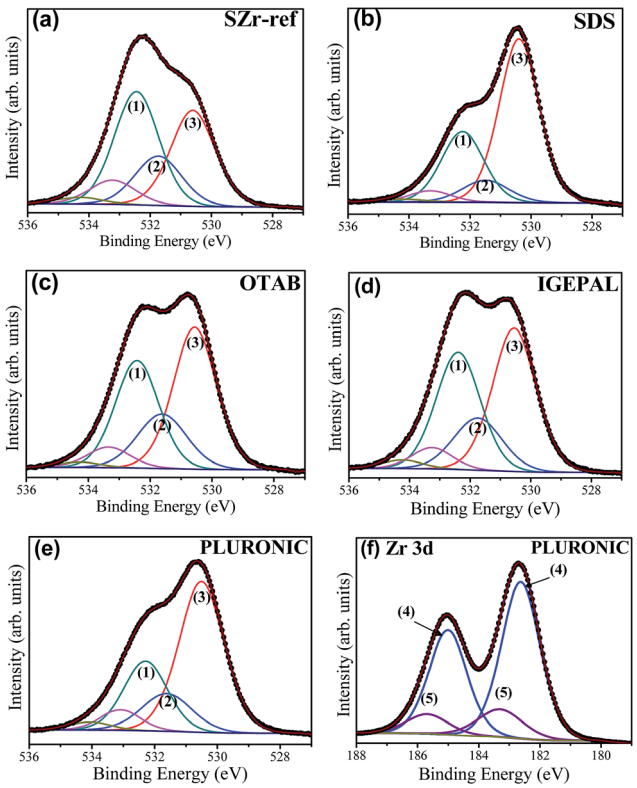


Fig. 6 (a)–(e) Deconvoluted XPS O 1s spectra of all samples with components attributed to: (1) $ZrO_x$–$SO_4$; (2) $ZrO_x$–OH and (3) $ZrO_2$-bulk; and (f) Zr $3d_{5/2}/3d_{3/2}$ doublet of the sample prepared with PLURONIC with sub-peaks assigned to: (4) $ZrO_2$-bulk and (5) sulfated zirconia.

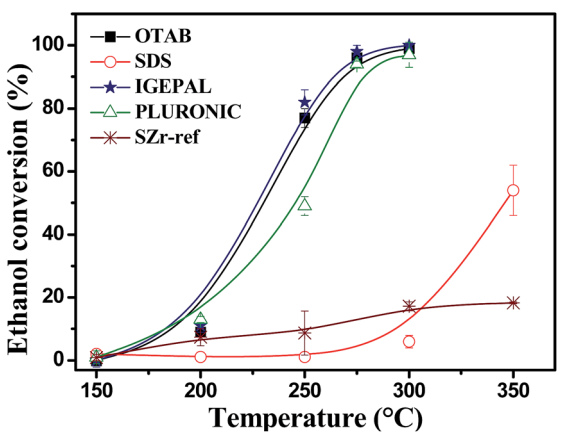


Fig. 7 Ethanol conversion as a function of temperature catalyzed by sulfated zirconia foams.

evaluated in function of reaction time at 250 °C (ESI Fig. S4†) and presented a quite good conversion stability up to 1 h under ethanol stream. Although the foam prepared with PLURONIC had the highest surface area (105 $m^2$ $g^{-1}$), the smaller pore volume and lower sulfur amount induced the slightly lower conversion of ethanol in the intermediate (between 200 and 275 °C) temperature range. In ESI is depicted the ethanol conversion on a nonsulfated commercial $ZrO_2$ reference (ESI Fig. S5†). The conversion is below 5% at all temperatures. Nevertheless, the samples prepared with the cationic and neutral surfactants OTAB, IGEPAL and PLURONIC allow to a total conversion of ethanol to ethene (Fig. 7) at 300 °C. The product formation rate of ethene, diethyl ether and acetaldehyde during the ethanol conversion reaction as a function of the temperature for the ceramic foam prepared with different surfactants were further shown in the Fig. S6 of the ESI.† Other byproducts were not detected. Consequently, the catalytic activity clearly depends on the combined effect of a hierarchical porous structure and a large number of active sites, which can be effectively accessed during the reaction.

## 4. Conclusions

The aeration process of zirconia sols is a promising route to prepare ceramic foams showing high porosity and hierarchical structure of pores sizes. It was demonstrated the versatility of the sol–gel process to design different ceramic foams morphologies by appropriate choice of the used surfactants. The main differences in the porous structure are related to the use of ionic or non-ionic surfactants that provides foams with high porosity and low surface area in the case of the ionic molecules and the opposite for non-ionic ones. The presence of a hierarchical macro–mesopores structure was observed for all the surfactants except the SDS one. The latter has led to foam with the higher porosity but only modal macropore family. Structural and surface characterizations of the samples showed the high amount of tetragonal phase and both the sulfate and hydroxyls groups on the surface. This feature evidences the potential of these ceramic foams as a catalyst. Ethanol dehydration reactions have revealed that samples presented the better catalytic performance when more active acid sites are available to promote the reaction, *i.e.*, combining high surface area, porosity and amount of acid sites. This behavior was achieved for the porous ceramics prepared using OTAB, IGEPAL and PLURONIC surfactants. Therefore, the porous characteristics associated to the surface properties make the macro–mesoporous sulfated zirconia foam a good catalyst for reactions requiring strong acid sites.

## Acknowledgements

This work was supported by the CAPES, CNPq and FAPESP agencies.

## References

1 G. L. Drisko, V. Luca, E. Sizgek, N. Scales and R. A. Caruso, *Langmuir*, 2009, **25**, 5286–5293.
2 S. Costacurta, L. Biasetto, E. Pippel, J. Woltersdorf and P. Colombo, *J. Am. Ceram. Soc.*, 2007, **90**, 2172–2177.
3 A. R. Studart, J. Studer, L. Xu, K. Yoon, H. C. Shum and D. A. Weitz, *Langmuir*, 2011, **27**, 955–964.
4 L. Martins, D. Cardoso, P. Hammer, T. Garetto, S. H. Pulcinelli and C. V. Santilli, *Appl. Catal., A*, 2011, **398**, 59–65.
5 R. Backov, *Soft Matter*, 2006, **2**, 452–464.
6 M. Faustini, D. Grosso, C. Boissière, R. Backov and C. Sanchez, *J. Sol-Gel Sci. Technol.*, 2014, **70**, 216–226.
7 J. Yang, J. Yu and Y. Huang, *J. Eur. Ceram. Soc.*, 2011, **31**, 2569–2591.
8 M. A. Alves-Rosa, L. Martins, S. H. Pulcinelli and C. V. Santilli, *Soft Matter*, 2013, **9**, 550–558.
9 L. Martins, M. A. A. Rosa, S. H. Pulcinelli and C. V. Santilli, *Microporous Mesoporous Mater.*, 2010, **132**, 268–275.
10 M. A. Alves-Rosa, L. Martins, P. Hammer, S. Pulcinelli and C. Santilli, *J. Sol-Gel Sci. Technol.*, 2014, **72**, 252–259.
11 C. C. Beozzo, M. A. Alves-Rosa, S. H. Pulcinelli and C. V. Santilli, *Materials*, 2013, **6**, 1967–1979.
12 F. Carn, A. Colin, M. F. Achard, H. Deleuze, C. Sanchez and R. Backov, *Adv. Mater.*, 2005, **17**, 62–66.
13 R. F. Lins, M. A. Alves-Rosa, S. H. Pulcinelli and C. V. Santilli, *J. Sol-Gel Sci. Technol.*, 2012, **63**, 224–229.
14 M. Wang, H. Y. Du, A. R. Guo, R. H. Hao and Z. G. Hou, *Mater. Lett.*, 2012, **88**, 97–100.
15 C. Lesaint, G. Kleppa, D. Arla, W. R. Glomm and G. Øye, *Microporous Mesoporous Mater.*, 2009, **119**, 245–251.
16 G. D. Yadav and J. J. Nair, *Microporous Mesoporous Mater.*, 1999, **33**, 1–48.
17 F. Cavani, S. Guidetti, L. Marinelli, M. Piccinini, E. Ghedini and M. Signoretto, *Appl. Catal., B*, 2010, **100**, 197–204.
18 A. A. Said, M. M. Abd El-Wahab and M. Abd El-Aal, *J. Mol. Catal. A: Chem.*, 2014, **394**, 40–47.
19 R. A. Comelli, C. R. Vera and J. M. Parera, *J. Catal.*, 1995, **151**, 96–101.
20 S. Ardizzone, C. L. Bianchi, G. Cappelletti and F. Porta, *J. Catal.*, 2004, **227**, 470–478.
21 A. I. Ahmed, S. A. El-Hakam, S. E. Samra, A. A. El-Khouly and A. S. Khder, *Colloids Surf., A*, 2008, **317**, 62–70.
22 L. A. Chiavacci, C. V. Santilli, S. H. Pulcinelli, C. Bourgaux and V. Briois, *Chem. Mater.*, 2004, **16**, 3995–4004.
23 E. W. Washburn, *Phys. Rev.*, 1921, **17**, 273–283.
24 S. J. Gregg and K. S. W. Sing, *Adsorption, Surface Area and Porosity*, Academic Press, London, 2nd edn, 1997.
25 M. A. A. Rosa, C. S. S. Sanhueza, C. V. Santilli, S. H. Pulcinelli and V. Briois, *J. Phys. Chem. B*, 2008, **112**, 9006–9012.
26 D. Myers, *Surfactant Science and Technology*, Wiley-Interscience, Hoboken, 2006.
27 M. Yashima, M. Kakihana and M. Yoshimura, *Solid State Ionics*, 1996, **86–8**, 1131–1149.
28 R. C. Garvie, R. H. Hannink and R. T. Pascoe, *Nature*, 1975, **258**, 703–704.
29 W. Li, H. Huang, H. Li, W. Zhang and H. Liu, *Langmuir*, 2008, **24**, 8358–8366.
30 A. Clearfield, G. P. D. Serrette and A. H. Khazisyed, *Catal. Today*, 1994, **20**, 295–312.

31 M. Hino, M. Kurashige, H. Matsuhashi and K. Arata, *Thermochim. Acta*, 2006, **441**, 35–41.
32 G. C. Boskovic, A. R. Zarubica, M. N. Kovacevic and P. S. Putanov, *J. Therm. Anal. Calorim.*, 2008, **91**, 849–854.
33 J. I. Di Cosimo, V. K. Diez, M. Xu, E. Iglesia and C. R. Apesteguia, *J. Catal.*, 1998, **178**, 499–510.
34 C. L. Bianchi, S. Ardizzone and G. Cappelletti, *Surf. Interface Anal.*, 2004, **36**, 745–748.
35 A. V. Naumkin, A. Kraut-Vass, S. W. Gaarestroom and C. J. Powell, *NIST X-ray Photoelectron Spectroscopy Database, NIST Standard Reference Database 20*, Version 4.1, created June 06 2000, last updated 15 2012, available from http://srdata.nist.gov/XPS/.

 